Desalination and Water Treatment
www.deswater.com
doi: 10.5004/dwt.2021.27911

242 (2021) 1–11
December

Nanometer and micrometer particle occurrence in the feed-concentrate channels of a nanofiltration membrane process

Courtney Powell, Steven J. Duranceau*

Department of Civil, Environmental, and Construction Engineering, University of Central Florida, 12800 Pegasus Drive, Suite 211, Orlando, FL 32816-2450, USA, Tel. +1-407-823-1440; email: steven.duranceau@ucf.edu (S.J. Duranceau)

Received 20 September 2021; Accepted 24 October 2021

ABSTRACT

The occurrence of submicron and micron-ranged particles in the feed-concentrate channels of an operating, production-capacity nanofiltration (NF) membrane process was investigated in this work. Nanoparticle tracking analysis and single-particle optical sensing technologies were utilized to evaluate the size (average diameter), distribution, and concentration of particles in the feed, interstage, and concentrate streams of a NF membrane process. Particles ranging between 50 nm and 70 μm were detected in the NF membrane feed-concentrate channel, and most of the particles identified had an average diameter of less than 1 μm. Submicron particle content averaged 64 million, 47 million, and 3.5 million particles/mL in the feed, interstage and concentrate streams, respectively. The concentration of particles less than 500 nm exceeded those greater than 500 nm by at least one order of magnitude. However, the less abundant microparticles occupied more of the volume within the feed-concentrate channel than the more concentrated submicron particles. The presence of particles larger than 5.0 microns, which is the nominal rating of the cartridge filters used in the plant's pretreatment process, were identified in each stream, some of which were on the order of 30–70 microns. Energy-dispersive X-ray spectroscopy was utilized to analyze the particles retained after filtering 20 L of the feed, interstage and concentrate streams through 0.2 microns rated 47 mm silver membranes. The results revealed deposits of calcium carbonate, elemental sulfur, and silts/clays in each stream; however, deposits of organic-based matter were mainly identified in the interstage and concentrate streams.

Keywords: Nanometer; Micrometer; Particles; Nanofiltration; Feed-concentrate channel; Single-particle optical sensing; Light obscuration; Nanoparticle tracking analysis

1. Introduction

It is well known that nanoparticles (NPs) from both natural and anthropogenic sources have been detected in the environment, primarily in surface water supplies [1–5]. The term 'nanoparticle' describes a subset of colloidal particles between 1 and 100 nm that typically possess a negative electrostatic surface charge [2,6,7]. NPs occur in various compositions and conformations and usually have large specific surface areas [8]. Naturally occurring nanoparticles (NNPs) arise from various sources, such as mineral weathering, and are prevalent in natural environments including groundwaters and surface waters which supply drinking water treatment plants (WTPs) [5]. Drinking water itself has been found to contain polydisperse, nanoscopic and microscopic solid and colloidal materials of irregular shape, often comprised of calcium carbonate and calcium sulfate [1]. Anthropogenic nanoparticles (ANPs) have also been detected in potable water sources; however, they are predicted to occur at significantly lower concentrations than NNPs based on empirical and mechanistic modeling of surface waters [3,4]. ANPs can enter aquatic environments through their use in products and industrial applications [9–12]. Although low levels of some microplastics

* Corresponding author.

have been detected in some karst aquifers and springs [13], it is generally acknowledged that non-karst groundwater supplies are predominantly absent of ANPs [10,14].

The removal of NPs, particularly ANPs in water treatment has been the focus of several studies due to concern about the potential toxicity of certain manufactured NPs. Although ANPs are present in low concentrations, their increasing use in products and applications will likely result in greater concentrations of manufactured NPs in surface water WTP supplies [10,11,15]. At the time of this writing, the USEPA has no monitoring guidelines for drinking WTPs on nanomaterials. Elements found in some ANPs are subject to regulatory limits; although, the maximum contaminant levels are far greater than the predicted concentrations of these types of particles [3,4].

Nanofiltration is a membrane liquid separation technology engineered for use in water treatment and has similar properties to reverse osmosis (RO) in that diffusion, electrostatic repulsion, and size exclusion are the principal mechanisms for solute separation [16–28]. Nanofiltration (NF) membranes are typically configured as spiral-wound, thin-film composite modules; are operated at lower feed pressures than RO; offer selective solute rejection based on both size and charge. They are often referred to as 'membrane softening' technologies for their ability to effectively remove calcium and magnesium hardness, as well as color, synthetic organic chemicals, and disinfection by-product precursors (natural organic matter) [16,21,27,29].

As water flows across the membrane channels, dissolved solids are rejected, and a boundary layer forms near the membrane surface in which the dissolved solids concentration exceeds the content in the bulk solution. To keep the membrane leaves separated and allow water to flow through the channel, a spacer net is inserted to promote turbulence and reduce the foulants that build upon the membrane surface [30–32]. The colloidal matter that can pass through the 5 μm nominal-rated polypropylene cartridge filters, which are typically used in the pretreatment process, has been shown to deposit onto the membrane surface [33–35].

It has been demonstrated that NPs are removed from drinking water supplies using synthetic nanofiltration (NF) membranes [36–39]. NPs that are present in the feed-concentrate stream cannot pass through the membrane as they are not dissolved, unlike soluble matter that can permeate based on diffusion due to a concentration gradient. For example, Sousa and Teixeira [37] determined that NF membranes completely removed particulate NPs, along with 92% of dissolved silver (Ag) ions particulate under laboratory conditions. Ionic strength, natural organic matter (NOM), and surface chemistry were shown to influence the removal of the dissolved Ag NPs [37]. An investigation by Van Koetsem et al. [39] corroborated the ability of membranes to remove NPs when the effective pore size exceeded the size of the ANP. Others have shown complete removal of NPs using NF membranes under lab and bench-scale conditions [24,29,40]. Furthermore, Fang and Duranceau [40] studied the impact of nanoparticles and surface morphology on RO and NF membrane productivity in bench-scale experiments and found that NPs can be trapped within the ridge-and-valley morphology of polyamide membranes which causes a resistance to flow.

Several studies have investigated the impact of hydraulic conditions and feed channel spacer geometry, orientation, and type on particle deposition [35,41–46]; however, it does not appear that any studies have been performed that provide insight into the occurrence of particles of any size range in NF feed-concentrate channels. The objective of this research was to determine the size distribution and concentration of submicron particles and microparticles in the feed-concentrate channel of an operating NF membrane process. The collected information regarding particle occurrence may provide additional insight into feed-concentrate channel dynamics and a greater understanding of how to best identify and diagnose the limitations of pretreatment and subsequent impacts on NF WTP process operations.

2. Experimental methods

2.1. Nanofiltration WTP description

Samples were collected from the feed, interstage, and concentrate stream (aqueous and filtered solids) of a full-scale nanofiltration membrane process at the City of Boynton Beach (City's) West WTP. The City's WTP can produce up to 8.7 million gallons/d of treated water (permeate) and is supplied by 11 groundwater wells in proximity to the facility. Pretreatment for the NF membrane process consists of pH acidification with sulfuric acid, scale inhibitor addition, and cartridge filtration (CF) using string wound 5 μm (nominal) rated filter elements. The nanofiltration membrane process configuration consists of six, two-stage membrane skids in parallel with six elements per pressure vessel. Dow NF 90-400 membranes are loaded in the first stage, and Dow NF 270-400 membranes are utilized in the second stage. Each train has a production capacity of 1.45 MGD, and the process operates at a recovery of 85%. Approximately 1.6 mg/L of NALCO™ PC-1850T scale inhibitor (Naperville, IL) with patented fluorescent tracking capabilities is added prior to membrane treatment to prevent the scaling of sparingly soluble salts in the concentrate channel that would otherwise foul the membrane surface. Typical water quality (average) for the NF feed, interstage and concentrate streams is presented in Table 1.

2.2. Sample collection and analysis

To assess the size and number of particles that occur in the membrane feed-concentrate channel, multiple 125 mL samples were collected from the NF process feed, interstage, and concentrate streams and submitted for particle size distribution analysis. Permeate water was not subject to analysis as particulate NPs do not permeate NF membranes. In addition, a pressure-controlled filtration apparatus commonly used to collect silt density index measurements was modified to filter 20 L of feed, interstage, and concentrate process streams to capture suspended material. Samples were filtered using 47 mm, 0.2 micron rated silver membrane filter pads (Sterlitech, Kent, WA).

The ability to access commercially available technologies to identify submicron particle size distribution tracking technologies and other sophisticated analytical equipment has expanded in recent years. Two technologies were

Table 1
Nanofiltration process feed and concentrate average water quality

Parameter (ion)	Feed (mg/L)	Interstage (mg/L)	Concentrate (mg/L)
Barium (Ba)	0.02	0.05	0.10
Calcium (Ca)	94.0	248	443
Magnesium (Mg)	2.40	2.90	5.40
Sodium (Na)	25.8	65.3	91.4
Strontium (Sr)	1.10	2.90	5.40
Bicarbonate (HCO_3)	228	596	977
Sulfate (SO_4)	57.8	154	375
Chloride (Cl)	39.0	98.2	117
Silicon dioxide (SiO_2)	13.4	34.8	46.2
Total dissolved solids	464	1,210	2,080
pH	6.8	7.2	7.3

utilized in this study to collect information on aqueous process streams: (1) nanoparticle tracking analysis (NTA); and (2) single-particle optical sensing (SPOS). To analyze filtered solids collected on the silver membrane filter pads, scanning electron microscopy (SEM) using energy-dispersive X-ray spectroscopy (EDS) and superimposed elemental imaging (SEI) were employed.

2.3. Nanoparticle tracking analysis

The average diameter and concentration of submicron particles in the samples collected from the West WTP were determined using the NanoSight NS300 (Malvern Panalytical, Worcestershire, United Kingdom). NTA technology utilizes light scattering and Brownian motion to generate high-resolution particle size distributions on a number-weighted basis for nano-sized materials in an aqueous medium within a specialized cell. In NTA, particles in an aqueous medium are illuminated through their interaction with a highly focused laser, by scattering incident light, as points of light moving under Brownian motion. Smaller particles move more quickly than larger particles and scatter less light. A camera mounted to a 20x magnification microscope is used to visualize the particles and track the movement of each particle over time to determine the diffusional rate. From the diffusional rate, the hydrodynamic diameter of each particle is quantified by the Stokes–Einstein equation using the NanoSight NTA analytical software to produce a high-resolution particle size distribution [47]. The known cell volume and the individual tracking of each particle allow for the simultaneous determination of particle concentration.

10, 5 min measurements were recorded for each sample. The NanoSight NS300 has an approximate (sample-dependent) working range of 30–1,000 nm and an optimum particle concentration of approximately 10^6–10^9 particles/mL. The instrument conformed to the 2018 ASTM E2834-12 [48] and is equipped with the manufacturer's concentration measurement upgrade; however, the accuracy of the concentration measurement cannot be verified as no NIST traceable particle concentration reference material is available at this time. The temperature of the sample was kept constant at 25°C. Table 2 details the specifications for the NanoSight NS300.

2.4. Single-particle optical sensing

The size distribution and concentration for particles in samples collected from the feed, interstage, and concentrate streams ranging from 0.5 to 400 μm was generated using the AccuSizer® A7000 AD equipped with the LE400 Sensor (PSS, Newcastle, England). SPOS technology utilizes two physical principles of detection depending on particle size: light obscuration for particles larger than 1.5 μm and light scattering for particles smaller than 1.5 μm. A dilute suspension of particles is passed through a region of uniform illumination produced by a laser diode. Particles greater the 1.5 μm are detected by the amount of light they obscure to the extinction detector, while particles less than 1.5 μm are detected by the intensity of light scattered at a range of angles towards a separate detector. In light scattering, the particle size is quantified by comparing the pulse heights to a calibration curve generated with standard reference materials of known size on the basis of circular equivalent diameter [49].

SPOS data can be reported in two formats: number weighted differential frequency (count or frequency) and volume-weighted percentage. The instrument conformed to the International Organization for Standardization (ISO) 21501-2:2019 and ISO 21501-3:2019 determination of particle size distribution guidelines [50,51].

2.5. Scanning electron microscopy, energy-dispersive X-ray analysis and superimposed elemental imaging®

SEM together with EDS and superimposed elemental imaging (SEI®) analysis was used to identify and quantify the elemental composition of solids collected on 0.2 micron, 47 mm silver membranes after filtering 20 L of feed, interstage, and concentrate. EDS analysis is generally performed together with electron microscopy to identify and quantify the elemental composition of a sample surface. The sample material is bombarded with electrons from an SEM which produces X-rays. The produced

Table 2
NanoSight NS300 specifications

Characteristic	Value
Analysis range	30 nm–1 μm
Concentration range	10^6–10^9 particles/mL

X-rays are then measured by an X-ray dispersive spectrometer. Every chemical element has its own characteristic wavelength by which it can be identified. SEI® is an X-ray excitation spectrum-based analysis with corresponding layered images showing the composition of specific inorganic particles.

The collected sample material was bombarded with electrons from a SU5000 SEM (Hitachi, Tokyo, Japan) to produce X-rays. The emitter used was a Schottky-type device with a spatial resolution of 2.0 nm at 1 kV and a high probe current (>200 mA). The resulting X-rays were then measured by the XFlash 6-60 dispersive spectrometer (Bruker, Billerica, MA) to acquire the elemental compositions (EDS spectra) of the samples. EDS spectra were collected on the filtered solids at each process location and quantified by atomic percentage. SEI® was incorporated into the analysis to visually distinguish the elemental composition of each compound on the surface by elemental mapping to enhance the findings from EDS to identify the chemical compositions of suspended solids, foulants and scales on the silver filter pad surfaces.

3. Results and discussion

3.1. Submicron particle observations by NTA

NTA data was collected for the NF feed, interstage, and concentrate process streams between December 2020 and April 2021. Due to the ability to track individual particles, the NTA instrument produces a number-weighted distribution in which each particle has an equal weighting once the final distribution is generated. For example, one particle at 100 nm will have just as much impact on the number weighted distribution as one particle at 1,000 nm. Since the volume of sample used is also known, sample concentration can be measured. To reduce the variances that may occur in samples that have low particle concentrations, at least ten reads for each sample were performed.

Table 3 provides information regarding the concentration of submicron particles for each of the three sampling locations. The number of particles in the feed-concentrate streams are on the order of a million particles per milliliter, and the quantities vary both in location and time indicating the dynamic nature of the flow across the membrane surface for this feed water supply. However, the particle concentrations in the NF concentrate among the sampling events were comparable in contrast to the fluctuations observed among the concentrations in the feed and interstage streams. Although the amount of naturally-occurring nanoparticles present in groundwater supplies has not been fully studied nor reported [3], the results collected in this work appear reasonable according to Filella et al. [52] who found between 2 and 12 million particles/mL ranging between 100 nm and 2 μm in water percolating through a geologic system. Also, research by Schiperski et al. [53] appeared to provide comparable results as they identified millions of particles/mL ranging between 0.5 and 150 μm at a karst spring during a snowmelt event.

Table 3
Nanoparticle tracking analysis particle concentration summary (particles/mL)

Sample date	Feed	Interstage	Concentrate
December 2020	4.75 (10E6)	4.95 (10E6)	2.84 (10E6)
January 2021	6.21 (10E6)	1.78 (10E8)	3.69 (10E6)
February 2021	2.40 (10E8)	2.11 (10E6)	3.46 (10E6)
April 2021	2.90 (10E6)	3.76 (10E6)	3.83 (10E6)
Mean	6.35 (10E7)	4.72 (10E7)	3.46 (10E6)
Standard deviation	1.98 (10E7)	1.01 (10E7)	7.05 (10E5)

Fig. 1 depicts an example of the NTA graphical results, presented as an overlay of the multiple measurements, showing the distribution by the average diameter of submicron particles per milliliter in the sample collected from the feed stream in January 2021. For this sample, the particles ranged in size from approximately 50–500 nm with a mean of 180 nm (Table 4). The samples varied in content (particles/mL) and size (nm) for each data collection event and by sample location. Despite variation among the samples, the overall data indicated that the average size of submicron particles fell within a narrow range, approximately 185 nm +/– 27 nm. Fig. 2 illustrates the averaged results of the measurements shown in Fig. 1 with the red shading indicating (+/–) one standard error of the mean, which can be found in Table 4. The shaded region illustrates the variance within the data set by size.

Table 4 provides a summary of the results for the NTA evaluation of the overall statistical data set obtained in this evaluation. The information is presented in terms of particle size, plus (+) or minus (–) the standard error for each date samples were collected and analyzed. Specific data collected and presented include the mean, standard deviation, and the point on the distribution curve below which 10%, 50%, and 90% of the particles fall within each analysis. These results correspond to the findings of Brant et al. [54] investigating the occurrence and composition of particulates in conventional filter process streams. It was shown based on a mass basis, inorganic and organic materials in the filter effluent streams were present as particles with diameters between 30 and 450 nm, regardless of whether direct or conventional filtration was used [54].

3.2. Microparticle examination by SPOS

SPOS data was also collected for NF feed, interstage, and concentrate process streams between December 2020 and April 2021 and analyzed by a particle counter capable of determining both particle size and concentration of suspensions. The SPOS analyzer had a detection range of 0.5 to 400 μm, and the data is presented on the basis of circular equivalent diameter. Since SPOS analyzers generate an intensity-weighted distribution (true particle

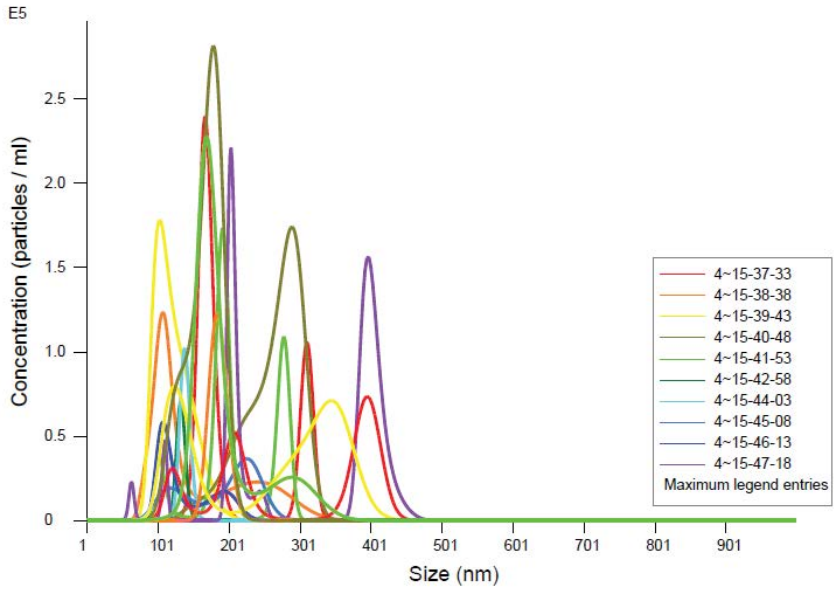

Fig. 1. Particle content (particles × E5/mL) as a function of size (nm) for feed sample (Jan. 2021).

Table 4
Nanoparticle tracking analysis statistical data summary by sample date

Sample date	Parameter	Feed (nm)	Interstage (nm)	Concentrate (nm)
December 2020	Mean	193 ± 13	107 ± 12	148 ± 20
	Standard deviation	63.0 ± 22	19.3 ± 5.7	29.9 ± 3.4
	d_{10}	98.1 ± 31	87.5 ± 8.1	116 ± 21
	d_{50}	189 ± 11	101 ± 11	152 ± 23
	d_{90}	253 ± 36	138 ± 19	177 ± 21
January 2021	Mean	180 ± 12	168 ± 39	197 ± 16
	Standard deviation	50.2 ± 9.2	98.4 ± 31	71.9 ± 17
	d_{10}	123 ± 7.7	70.3 ± 13	105 ± 13
	d_{50}	166 ± 11	137 ± 30	182 ± 14
	d_{90}	252 ± 23	299 ± 77	284 ± 37
February 2021	Mean	173 ± 22	170 ± 10	202 ± 43
	Standard deviation	59.5 ± 15	26.1 ± 11	99.4 ± 22
	d_{10}	105 ± 14	124 ± 21	87.6 ± 26
	d_{50}	168 ± 25	197 ± 10	207 ± 67
	d_{90}	253 ± 43	200 ± 22	323 ± 59
April 2021	Mean	248 ± 59	231 ± 35	207 ± 45
	Standard deviation	66.3 ± 25	71.6 ± 17	81.1 ± 23
	d_{10}	168 ± 43	135 ± 18	122 ± 31
	d_{50}	246 ± 65	253 ± 44	188 ± 48
	d_{90}	308 ± 75	301 ± 46	315 ± 68

counters), the particle size distributions are reported in two formats number (frequency) and volume. Table 5 provides the particle concentrations greater than or equal to 0.5 μm in each stream in number of particles per milliliter (mL). The concentration of microscale particles in the feed-concentrate streams determined by SPOS was less than the reported concentrations of submicron particles, specifically particles ranging from 50 nm to 500 nm, from NTA. The quantities differ both in sample location and in time (sampling event) indicating the dynamic nature of the feed water supplied by groundwater wells and the flow across the NF membrane surface.

Fig. 3 depicts the number weighted differential frequency histogram generated from the February 2021 interstage stream sample. This graph reveals the percentage of particles detected vs. the size of the particles detected, on a log scale,

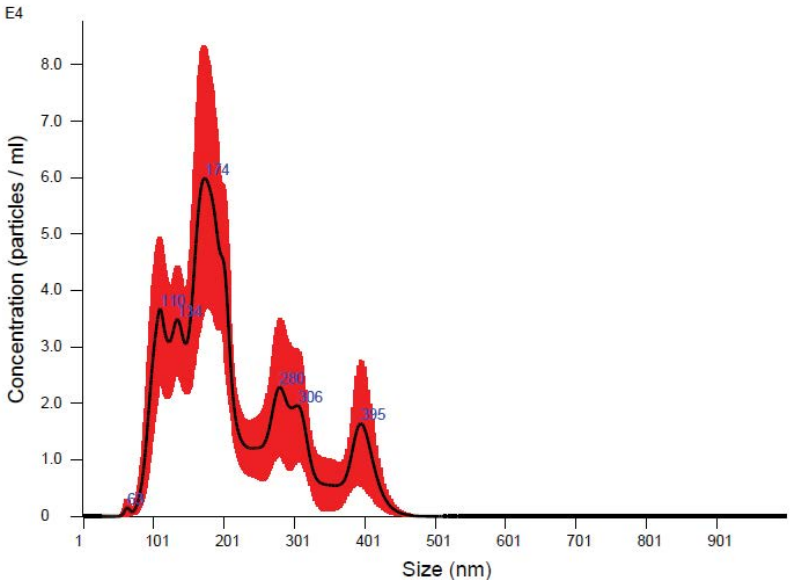

Fig. 2. Particle content (particles × E4/mL) as a function of size (nm) for feed sample (Jan. 2021).

Table 6
Number weighted mean particle size by SPOS

Sample date	Mean	Feed	Interstage	Concentrate
December 2020	Number weighted (μm)	0.82 ± 0.43	0.85 ± 0.63	0.76 ± 0.37
	Volume weighted (μm)	13.4 ± 14	11.6 ± 9.27	34.4 ± 30
January 2021	Number weighted (μm)	0.72 ± 0.42	0.69 ± 0.27	0.71 ± 0.42
	Volume weighted (μm)	97.8 ± 48	11.8 ± 10.0	67.4 ± 33
February 2021	Number weighted (μm)	0.66 ± 0.34	0.68 ± 0.62	0.60 ± 0.28
	Volume weighted (μm)	26.9 ± 20	22.8 ± 5.9	23.1 ± 15
April 2021	Number weighted (μm)	0.67 ± 0.44	0.66 ± 0.32	0.73 ± 0.44
	Volume weighted (μm)	36.7 ± 22	21.2 ± 14	41.4 ± 28
Total	Number weighted (μm)	0.72 ± 0.41	0.72 ± 0.46	0.70 ± 0.37
	Volume weighted (μm)	43.7 ± 26	16.9 ± 12	41.6 ± 26

where each particle has equal weighting. Furthermore, the number weighted particle distribution histogram presented in Fig. 3 for the interstage stream was representative of the number weighted distributions observed for each location throughout the different sampling events in that the majority of particles identified had an average diameter of less than 1 micron.

Fig. 4 provides the differential-volume percentage graph detailing the SPOS results of the sample collected from the interstage stream on February 2021. The volume data is generated based on the assumption that each particle is spherical. Since the volume of a particle increases proportionally to the diameter cubed, the volume data are inherently weighted towards the larger particles and better represent where the bulk or mass of the system lies. For example, roughly one million, 1-μm particles contribute the same volume percentage as one, 100-μm particle. Unlike the number weighted distribution which is heavily skewed to the smaller more abundant particles, the volume-weighted distribution is skewed to the less abundant microscale particles; therefore, the larger particles occupy noticeably more of the volume within the feed-concentrate channel than the submicron particles (<1.0 μm).

Table 6 presents the results of particle size measurements for the particle distributions identified by SPOS ranging between 0.5 and 400 μm. Overall, the average particle sizes determined from the number weighted distribution for each location were skewed towards the lower end of the detection limit, while the average sizes found from the volume-weighted distributions were noticeably larger. When considering the average results from both distributions, it was discovered that the average size of the particles in each of the three locations was similar for the number weighted distributions; however, the average size of the interstage particles in the volume-weighted distribution was found to be smaller than those in the feed and concentrate streams. Although, it is important to note

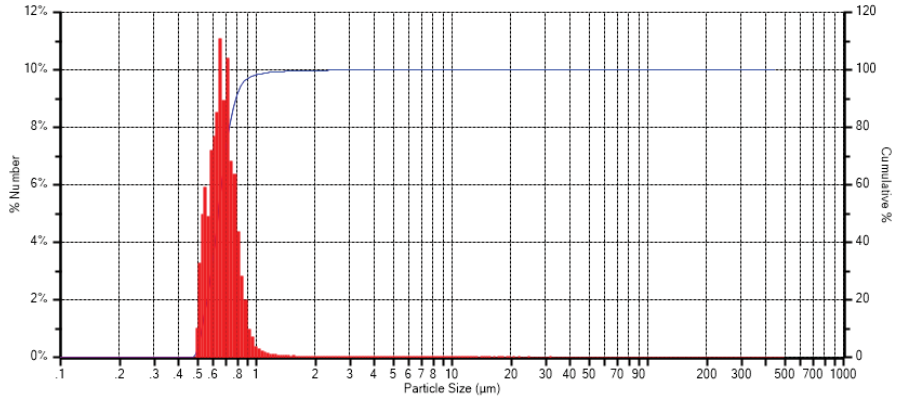

Fig. 3. Number weighted differential frequency histogram (Feb. 2021).

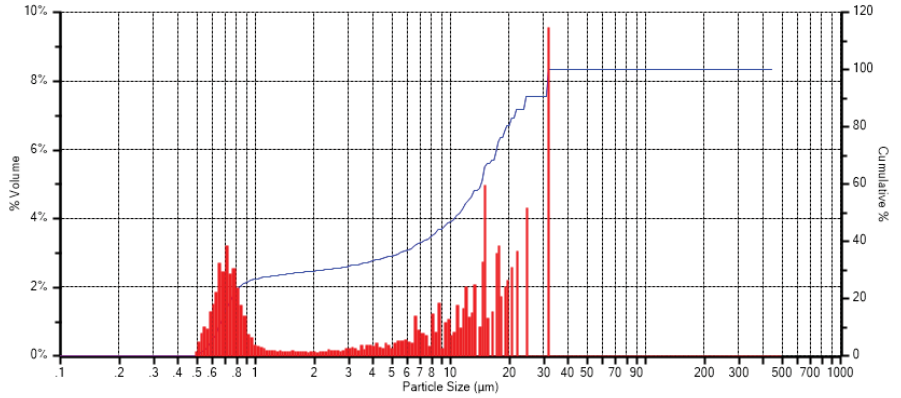

Fig. 4. Differential volume-weighted percentage of particles vs. particle size (Feb. 2021).

the measurements varied for each location both within a single data set and over the four data sets collected in this study.

3.3. Process bulk stream solids identification

The use of SEM and EDS with SEI techniques allowed for the identification of inorganic and organic solids that occur within the feed-concentrate channels of a NF membrane process. The silver membrane filters used to collect the suspended solids are shown in Fig. 5. Visual inspection of the membranes suggests that the composition of the foulants filtered from each stream is different as the three surfaces appear to have distinct coloring.

EDS spectra outputs from the analysis of the samples collected from the NF feed, interstage, and concentrate streams are presented in Table 7 and Fig. 6. Figs. 7–9 present elemental mapping of the collected material in the form of superimposed elemental imaging. The SEM, EDS, and SEI® results represent the composition of particles detected in the feed-concentrate channels. Particles from the feed stream predominantly consisted of calcium carbonate, elemental sulfur, and silts/clays. The interstage and concentrate streams contained particles that were comprised of organic-based matter, calcium carbonate, elemental sulfur, and silts/clays. Particle composition appears to be in agreement with the findings of Kaegi et al. [55].

Table 7
Quantified EDS results by atomic percentage

	Atomic percentage (%)		
Element	Feed	Interstage	Concentrate
Carbon	5.14	2.25	7.61
Oxygen	52.6	53.0	52.8
Silicon	9.65	20.9	20.7
Calcium	7.49	<0.2	3.91
Silver	23.5	22.1	11.6
Sulfur	1.73	1.72	0.81
Aluminum	<0.2	ND	2.54
Phosphorus	ND	ND	<0.2

ND: not detected

3.4. Occurrence of organic and inorganic colloids and particulates

In-situ microscopic observations have been used in prior investigations on particle deposition, in addition to organic and biofilm monitoring, but have been primarily limited to laboratory-scale experiments. The results indicate that a wide range of particulates, in terms of both size and composition, flow across membrane surfaces which would demonstrate that studies that relied on particles of

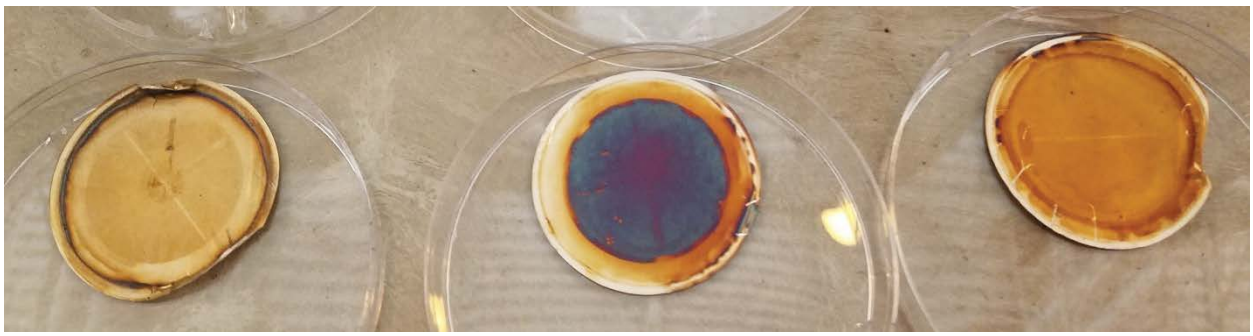

Fig. 5. Nanofiltration feed (left), interstage (center) and concentrate (right) collected filtrate deposits.

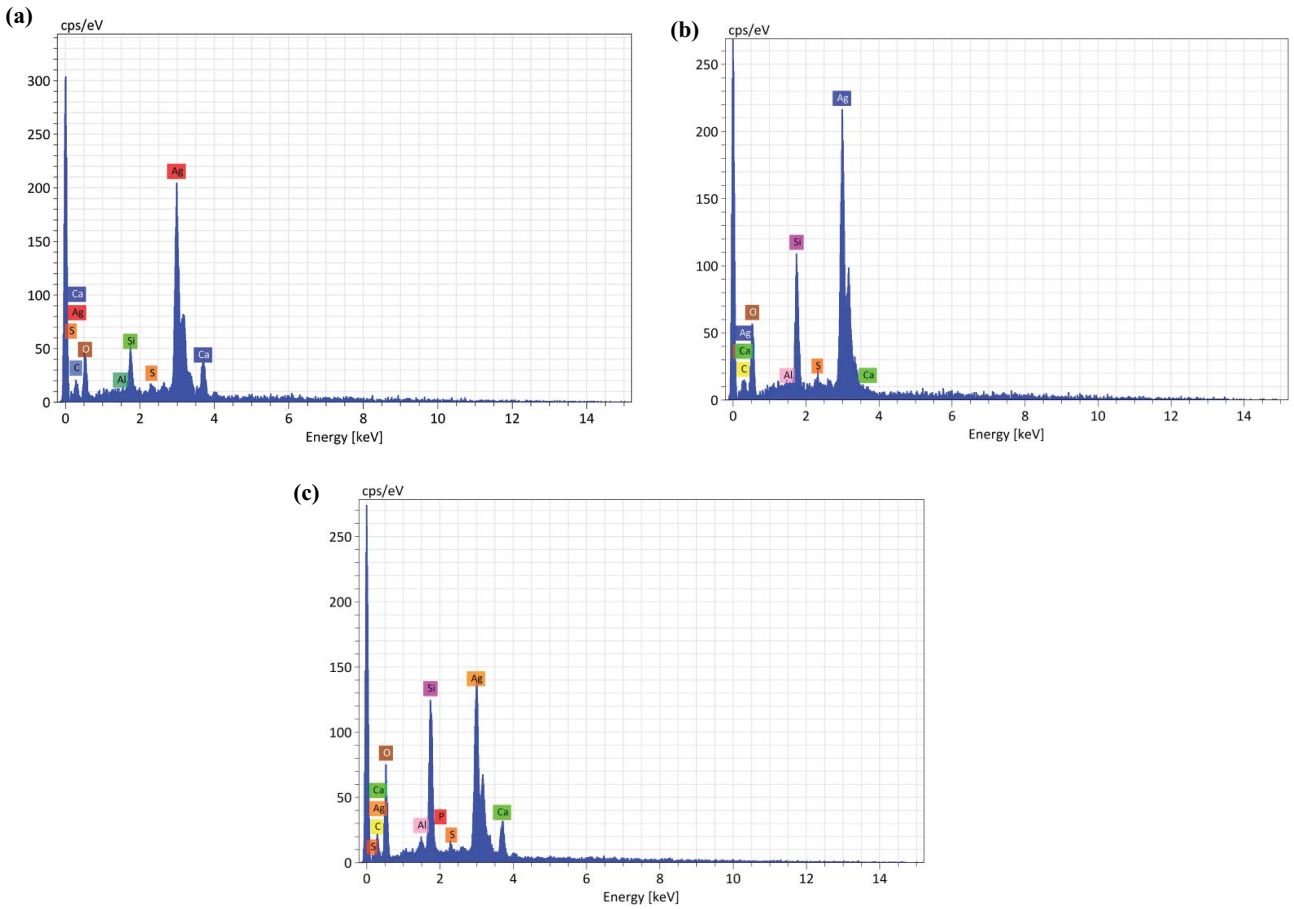

Fig. 6. EDS composition of (a) feed water, (b) interstage and (c) concentrate particulate deposits.

Table 5
SPOS particle concentration summary (particles/mL)

Sample date	Feed	Interstage	Concentrate
December 2020	1.02 (10E5)	4.67 (10E4)	1.56 (10E5)
January 2021	1.47 (10E5)	1.43 (10E5)	1.85 (10E5)
February 2021	1.44 (10E5)	3.53 (10E4)	2.53 (10E5)
April 2021	1.13 (10E5)	1.51 (10E5)	1.23 (10E5)
Mean	1.27 (10E5)	9.40 (10E4)	1.79 (10E5)
Standard deviation	2.24 (10E4)	6.15 (10E4)	5.53 (10E4)

a specific size and type, such as the work performed by Neal et al. [41], may not reflect conditions found in practice. Chemical analyses of the full-scale NF bulk feed, interstage, and concentrate streams revealed the presence of organic and inorganic colloids. Colloidal matter refers to mixtures in which microscopically dispersed insoluble particles of one substance are dispersed in another substance. The size of the suspended particles in a colloid can range from 1 to 1,000 nm, and the deposition of these colloidal particles on an RO or NF membrane is believed to form a cake layer, which can adversely affect the membrane

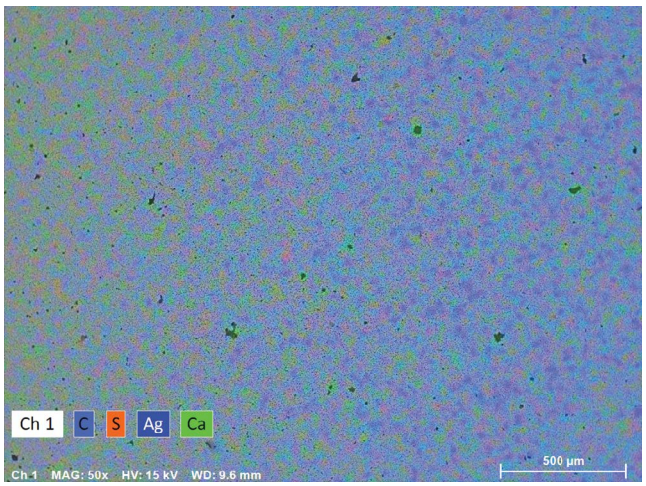

Fig. 7. Superimposed elemental imaging (SEI®): feed water calcium carbonate and elemental sulfur.

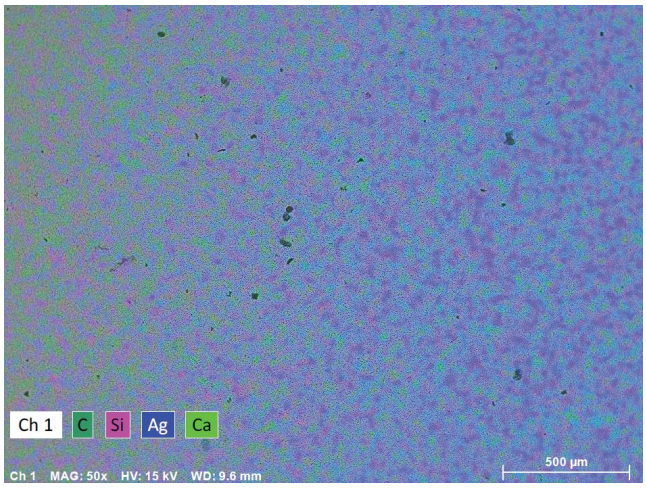

Fig. 8. Superimposed elemental imaging (SEI®): interstage stream organic-based matter, calcium carbonate, sulfur and silt/clays.

flux [16,34]. Natural organic matter has been shown to at times appear colloidal and foul membranes as higher concentrations of organic carbon are present in the concentrate [34,56].

These findings are supported by results from a previous study performed on a membrane element taken from a pilot study at the City's West WTP on October 24, 2019, prior to the bulk stream filtering sample events [57]. The foulant on the element's surface was found to consist of silts/clays, calcium sulfate, and organic-based matter using SEM and EDS along with Fourier-transform infrared (FTIR) spectroscopy. Loss on ignition results indicated that the foulant deposit consisted of approximately 78% organic content and 22 percent inorganic matter. Analysis of cartridge pre-filters from the same site found calcium sulfate as trapped particulates [57]. This implied that the trace calcium sulfate particles identified by SEM and FTIR spectroscopy entered the NF membrane feed-concentrate channel as suspended particles.

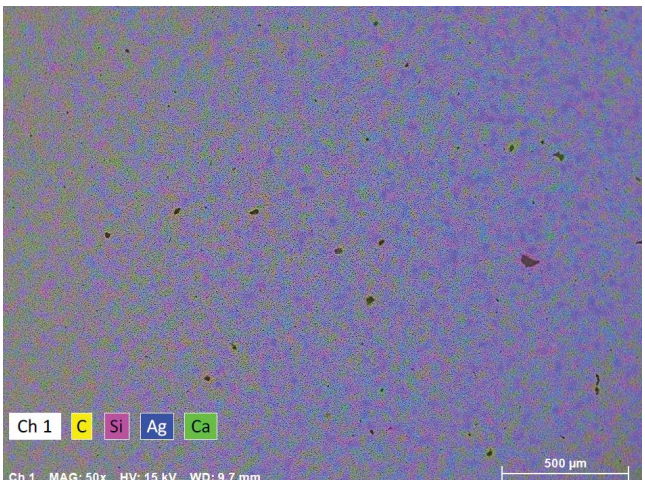

Fig. 9. Superimposed elemental imaging (SEI®): concentrate stream calcium carbonate and clays.

The fact remains that particles found in the full-scale NF plant's feed water were in fact larger than 5 µm, which is the nominal rating of the pretreatment system's cartridge filters. Furthermore, individual particles as large as 30 µm in the interstage stream and up to 70 µm in the concentrate stream were identified which could be explained by agglomeration within the feed-concentrate channel. Previous work has reported that colloids can detach over a wide range of flow rates in porous media in a distributed manner [58]. Additionally, hydrodynamic fluid conditions are provided by the spacer within the channel that could cause shearing which would provide the conditions for agglomeration and the subsequent formation of larger colloidal particles [35,59,60]. It is also possible that gypsum nucleation occurs resulting in the formation of large particles in the concentrate stream due to the concentration of calcium and sulfate in the presence of nanoparticles, as demonstrated by the work of Oshchepkov et al. [61], who showed that nanoparticles can play a role in sparingly soluble salts nucleating in the bulk aqueous solution. This would also possibly explain why the number of particles tends to be lower in the concentrate stream, as compared to the feed and interstage streams, perhaps because larger NPs could be depositing on the last few membranes in the tail-end of the full-scale process.

4. Conclusions

In this research, two different techniques were used to evaluate the particle size distribution and the concentration of submicron particles and microparticles present in the collected water samples. Additionally, the composition of particles collected from each sampling location was determined utilizing SEM and EDS with SEI. Submicron particles and microparticles were found in the feed-concentrate channels of a full-scale NF membrane process with the concentration of the former comfortably exceeding that of the latter throughout the system.

Particles ranging between 50 nm and 70 µm were detected in the NF membrane feed-concentrate channel;

most of the particles identified had an average diameter of less than 1 μm. Submicron particle content averaged 64 million, 47 million, and 3.5 million particles/mL in the feed, interstage and concentrate streams, respectively. The concentration of particles less than 500 nm exceeded those greater than 500 nm by at least one order of magnitude for each stream. However, the less abundant microparticles occupied noticeably more volume within the feed-concentrate channel than the submicron particles. Particles larger than 5.0 microns, which exceed the nominal rating of the plant's cartridge filters, were present in each stream, and a small number of particles identified were on the order of 30–70 microns.

EDS was utilized to identify the composition of particles in the feed, interstage and concentrate streams through 0.2 microns rated 47 mm silver membranes. The results revealed particulates comprised of deposits of calcium carbonate, elemental sulfur, and silts/clays, while organic-based matter deposits were mainly identified in the interstage and concentrate streams.

Acknowledgments

The research reported herein was funded, in part, on behalf of the City of Boynton Beach (Florida) and Globaltech (Boca Raton, FL) for funding this work (Project No. 1620-8233). We are thankful for the assistance of the operations staff located at the City's West Nanofiltration WTP. Additional funding was provided by UCF's Research Foundation's Jones Edmunds Fund 1620-8A22. The contributions of students in the Civil, Environmental and Construction Engineering Department's Water Quality Engineering Research Group, who assisted in fieldwork, were greatly appreciated. The opinions and findings expressed in this research are those of the authors and do not necessarily reflect the view of UCF (Orlando, FL), its Board of Governors, or its Research Foundation.

References

[1] S. Griffin, M.I. Masood, M.J. Nasim, M. Sarfraz, A.P. Ebokaiwe, K.-H. Schäfer, C.M. Keck, C. Jacob, Natural nanoparticles: a particular matter inspired by nature, Antioxidants, 7 (2017) 1–21.
[2] A. Hartland, J.R. Lead, V.I. Slaveykova, D. O'Carroll, E. Valsami-Jones, The environmental significance of natural nanoparticles, Nat. Educ. Knowl., 4 (2013) 1–7.
[3] P. Westerhoff, A. Atkinson, J. Fortner, M.S. Wong, J. Zimmerman, J. Gardea-Torresdey, J. Ranville, P. Herckes, Low risk posed by engineered and incidental nanoparticles in drinking water, Nat. Nanotechnol., 13 (2018) 661–669.
[4] K. Tiede, S.F. Hanssen, P. Westerhoff, G.J. Fern, S.M. Hankin, R.J. Aitken, Q. Chaudhry, A.B.A. Boxall, How important is drinking water exposure for the risks of engineered nanoparticles to consumers?, Nanotoxicology, 10 (2016) 102–110.
[5] N.S. Wigginton, K.L. Haus, M.F. Hochella Jr., Aquatic environmental nanoparticles, J. Environ. Monit., 9 (2007) 1306–1316.
[6] M.F. Hochella Jr., There's plenty of room at the bottom: nanoscience in geochemistry, Geochim. Cosmochim. Acta, 66 (2002) 735–743.
[7] E. Tipping, D.C. Higgins, The effect of adsorbed humic substances on the colloid stability of haematite particles, Colloids Surf., 5 (1982) 85–92.
[8] J.R. Lead, K.J. Wilkinson, Aquatic colloids and nanoparticles: current knowledge and future trends, Environ. Chem., 3 (2006) 159–171.
[9] S.R. Tangaa, H. Selck, M. Winther-Nielsen, F.R. Khan, Trophic transfer of metal-based nanoparticles in aquatic environments: a review and recommendations for future research focus, Environ. Sci. Nano, 3 (2016) 966–981.
[10] M. Troester, H.-J. Brauch, T. Hofmann, Vulnerability of drinking water supplies to engineered nanoparticles, Water Res., 96 (2016) 255–279.
[11] K.D. Good, L.E. Bergman, S.S. Klara, M.E. Leitch, J.M. VanBriesen, Implications of engineered nanomaterials on drinking water sources, J. Am. Water Works Assn., 108 (2016) E1–E17.
[12] M. Zhang, J. Yang, Z. Cai, Y. Feng, Y. Wang, D. Zhang, Z. Pan, Detection of engineered nanoparticles in aquatic environments: current status and challenges in enrichment, separation, and analysis, Environ. Sci. Nano, 6 (2019) 709–735.
[13] S.V. Panno, W.R. Kelly, R. Walton, J. Scott, Microplastic contamination in Karst groundwater systems, Groundwater, 57 (2019) 189–196.
[14] S.M. Mintenig, M.G.J. Löder, S. Primpke, G. Gerdts, Low numbers of microplastics detected in drinking water from ground water sources, Sci. Total Environ., 648 (2019) 631–635.
[15] V.S. Sousa, M.R. Teixeira, Metal-based engineered nanoparticles in the drinking water treatment systems: a critical review, Sci. Total Environ., 707 (2020) 136077.
[16] S.J. Duranceau, J.S. Taylor, Chapter 11 – Membrane Processes, J.K. Edzwald, Ed., Water Quality and Treatment, 6th ed., McGraw-Hill, New York, NY, 2011, pp. 11–1 to 11–106.
[17] B.J. Marinas, R.I. Urama, Modeling concentration-polarization in reverse osmosis spiral-wound elements, J. Environ. Eng., 122 (1996) 292–298.
[18] O. Kedem, A. Katchalsky, Thermodynamic analysis of the permeability of biological membranes to non-electrolytes, Biochim. Biophys. Acta, 27 (1958) 229–246.
[19] O. Kedem, A. Katchalsky, Permeability of composite membranes. Part 1.–Electric current, volume flow and flow of solute through membranes, Trans. Faraday Soc., 59 (1963) 1918–1930.
[20] K. Wesolowska, S. Koter, M. Bodzek, Modelling of nanofiltration in softening water, Desalination, 163 (2004) 137–151.
[21] S.J. Duranceau, J.S. Taylor, L.A. Mulford, SOC removal in a membrane softening process, J. Am. Water Works Assn., 84 (1992) 68–78.
[22] J.G. Wijmans, R.W. Baker, The solution-diffusion model: a review, J. Membr. Sci., 107 (1995) 1–21.
[23] T. Chaabane, S. Taha, M.T. Ahmed, R. Maachi, G. Dorange, Coupled model of film theory and the Nernst–Planck equation in nanofiltration, Desalination, 206 (2007) 424–432.
[24] W.R. Bowen, H. Mukhtar, Characterisation and prediction of separation performance of nanofiltration membranes, J. Membr. Sci., 112 (1996) 263–274.
[25] Y. Garba, S. Taha, N. Gondrexon, G. Dorange, Ion transport modelling through nanofiltration membranes, J. Membr. Sci., 160 (1999) 187–200.
[26] S.J. Duranceau, Modeling the permeate transient response to perturbations from steady state in a nanofiltration process, Desal. Water Treat., 1 (2009) 7–16.
[27] J.S. Taylor, J.A.M.H. Hofman, S.J. Duranceau, J.C. Kruithof, J.C. Schippers, Simplified modeling of diffusion controlled membrane systems, J. Water Supply Res. Technol. AQUA, 43 (1994) 238–245.
[28] S. Jeffery-Black, S.J. Duranceau, The influence of solute polarizability and molecular volume on the rejection of trace organics in loose nanofiltration membrane processes, Desal. Water Treat., 57 (2016) 29059–29069.
[29] B. van der Bruggen, C. Vandecasteele, Removal of pollutants from surface water and groundwater by nanofiltration: overview of possible applications in the drinking water industry, Environ. Pollut., 122 (2003) 435–445.
[30] V. Geraldes, V. Semiao, M.N. de Pinho, The effect of the ladder-type spacers configuration in NF spiral-wound modules on the concentration boundary layers disruption, Desalination, 146 (2002) 187–194.
[31] J.S. Vrouwenvelder, D.A. Graf von der Schulenburg, J.C. Kruithof, M.L. Johns, M.C.M. van Loosdrecht, Biofouling of

spiral-wound nanofiltration and reverse osmosis membranes: a feed spacer problem, Water Res., 43 (2009) 583–594.
[32] Y. Gao, S. Haavisto, C.Y. Tang, J. Salmela, W. Li, Characterization of fluid dynamics in spacer-filled channels for membrane filtration using Dopper optical coherence tomography, J. Membr. Sci., 448 (2013) 198–208.
[33] S.G. Yiantsios, D. Sioutopoulos, A.J. Karabelas, Colloidal fouling of RO membranes: an overview of key issues and efforts to develop improved prediction techniques, Desalination, 183 (2005) 257–272.
[34] C.Y. Tang, T.H. Chong, A.G. Fane, Colloidal interactions and fouling of NF and RO membranes: a review, Adv. Colloid Interface Sci., 164 (2011) 126–143.
[35] A.I. Radu, M.S.H. van Steen, J.S. Vrouwenvelder, M.C.M. van Loosdrecht, C. Picioreanu, Spacer geometry and particle deposition in spiral wound membrane feed channels, Water Res., 64 (2014) 160–176.
[36] T.E. Abbott Chalew, G.S. Ajmani, H. Huang, K.J. Schwab, Evaluating nanoparticle breakthrough during drinking water treatment, Environ. Health Perspect., 121 (2013) 1161–1166.
[37] V.S. Sousa, M.R. Teixeira, Silver nanoparticles separation from the water using nanofiltration membranes: the role of mono-divalent salts and NOM, Sep. Purif. Technol., 149 (2015) 165–173.
[38] D.A. Ladner, M. Steele, A. Weir, K. Hristovski, P. Westerhoff, Functionalized nanoparticle interactions with polymeric membranes, J. Hazard. Mater., 211–212 (2012) 288–295.
[39] F. Van Koetsem, S. Verstraete, E. Wallaert, K. Verbeken, P. Van der Meeren, J. Rinklebe, G. Du Laing, Use of filtration techniques to study environmental fate of engineered metallic nanoparticles: factors affecting filter performance, J. Hazard. Mater., 322 (2017) 105–117.
[40] Y. Fang, S. Duranceau, Study of the effect of nanoparticles and surface morphology on reverse osmosis and nanofiltration membrane productivity, Membranes, 3 (2013) 196–225.
[41] P.R. Neal, H. Li, A.G. Fane, D.E. Wiley, The effect of filament orientation on critical flux and particle deposition in spacer-filled channels, J. Membr. Sci., 214 (2003) 165–178.
[42] F. Li, W. Meindersma, A.B. De Haan, T. Reith, Optimization of commercial net spacers in spiral wound membrane modules, J. Membr. Sci., 208 (2002) 289–302.
[43] J. Schwinge, P.R. Neal, D.E. Wiley, D.F. Fletcher, A.G. Fane, Spiral wound modules and spacers: review and analysis, J. Membr. Sci., 242 (2004) 129–153.
[44] A.L. Ahmad, K.K. Lau, M.Z. Abu Bakar, Impact of different spacer filament geometries on concentration polarization control in narrow membrane channel, J. Membr. Sci., 262 (2005) 138–152.
[45] G. Guillen, E.M.V. Hoek, Modeling the impacts of feed spacer geometry on reverse osmosis and nanofiltration processes, Chem. Eng. J., 149 (2009) 221–231.
[46] S.S. Bucs, R.V. Linares, J.O. Marston, A.I. Radu, J.S. Vrouwenvelder, D. Picioreanu, Experimental and numerical characterization of the water flow in spacer-filled channels of spiral-wound membranes, Water Res., 87 (2015) 299–310.
[47] R. Xu, Light scattering: a review of particle characterization applications, Particuology, 18 (2015) 11–21.
[48] ASTM International, Standard Guide for Measurement of Particle Size Distribution of Nanomaterials in Suspension by Nanoparticle Tracking Analysis (NTA), American Society for Testing and Materials, West Chonshohocken, PA, 2018. Available at: https://compass.astm.org/Standards/HISTORICAL/E2834-12.htm
[49] B. Tolla, D. Boldridge, Distortion of single-particle optical sensing (SPOS) particle count by sub-countable particles, Part. Part. Syst. Char., 27 (2010) 21–31.
[50] International Organization for Standardization, ISO 21501-2:2019, Determination of Particle Size Distribution – Single Particle Light Interaction Methods – Part 2: Light Scattering Liquid-Borne Particle Counter, ISO Central Secretariat Ch. de Blandonnet 8 Case Postale 401 CH – 1214 Vernier, Geneva Switzerland, 2019. Available at: https://www.iso.org/standard/75048.html
[51] International Organization for Standardization, ISO 21501-3:2019, Determination of Particle Size Distribution – Single Particle Light Interaction Methods – Part 3: Light Extinction Liquid-Borne Particle Counter, ISO Central Secretariat Ch. de Blandonnet 8 Case Postale 401 CH – 1214 Vernier, Geneva Switzerland, 2019. Available at: https://www.iso.org/standard/75049.html
[52] M. Filella, V. Chanudet, S. Philippo, F. Quentel, Particle size and mineralogical composition of inorganic colloids in waters draining the adit of an abandoned mine, Geosdorf, Luxembourg, J. Appl. Geochem., 24 (2009) 52–61.
[53] F. Schiperski, J. Zirlewagen, O. Hillebrand, T. Licha, T. Scheytt, Preliminary results on the dynamics of particles and their size distribution at a karst spring during a snowmelt event, J. Hydrol., 524 (2015) 326–332.
[54] J.A. Brant, I. Koyuncu, H. LeCoane, S.V. Verrapaneni, M. Wiesner, Occurrence and composition of particulates in filter process streams, J. Am. Water Works Assn., 103 (2011) 46–60.
[55] R. Kaegi, T. Wagner, B. Hetzer, B. Sinnet, G. Tzvetkov, M. Boller, Size, number and chemical composition of nanosized particles in drinking water determined by analytical microscopy and LIBD, Water Res., 42 (2008) 2778–2786.
[56] S. Hong, M. Elimelech, Chemical and physical aspects of natural organic matter (NOM) fouling of nanofiltration membranes, J. Membr. Sci., 132 (1997) 159–181.
[57] American Water Chemicals, Analytical Testing Report for Boynton Beach 10/24/2019, 1802 Corporate Center Lane, Plant City, FL 33563, 2019.
[58] E.M. Hoek, A.S. Kim, M. Elimelech, Influence of crossflow membrane filter geometry and shear rate on colloidal fouling in reverse osmosis and nanofiltration separations, Environ. Eng. Sci., 19 (2002) 357–372.
[59] J. Bergendahl, D. Grasso, Prediction of colloid detachment in a model porous media: hydrodynamics, Chem. Eng. Sci., 55 (2000) 1523–1532.
[60] A.H. Haidari, S.G.J. Heijman, W.S.J. Uijttewaal, W.G.J. van der Meer, Determining the effect of spacer orientations on channel hydraulic conditions using PIV, J. Water Process Eng., 31 (2019) 100820.
[61] M. Oshchepkov, K. Popov, A. Kovalenko, A. Redchuk, J. Dikareva, I. Pochitalkina, Initial stages of gypsum nucleation: the role of "nano/microdust", Minerals, 10 (2020) 1083.